

## Numerical simulations of drumlin formation

Journal:	<i>Proceedings A</i>
Manuscript ID	RSPA-2017-0220.R1
Article Type:	Research
Date Submitted by the Author:	n/a
Complete List of Authors:	Fannon, James; University of Limerick, MACSI Fowler, Andrew; University of Limerick, MACSI Moyle, Iain; University of Limerick, MACSI
Subject:	Glaciology < EARTH SCIENCES, Mathematical modelling < MATHEMATICS
Keywords:	Drumlins, Ribbed moraine, Mega-scale glacial lineations, Instability theory
Subject Category:	Earth Science

SCHOLARONE™  
Manuscripts

# Numerical simulations of drumlin formation

J. S. Fannon<sup>1</sup>, A. C. Fowler<sup>1,2</sup>, and I. R. Moyses<sup>1</sup>

<sup>1</sup>MACSI, University of Limerick, Limerick, Ireland

<sup>2</sup>OCIAM, University of Oxford, Oxford, UK

July 21, 2017

## Abstract

We summarise the present form of the instability theory for drumlin formation, which describes the coupled subglacial flow of ice, water and sediment. This model has evolved over the last twenty years, and is now at the point where it can predict instabilities corresponding to ribbed moraine, drumlins and mega-scale glacial lineations (MSGSL), but efforts to provide numerical solutions of the model have been limited. The present summary adds some slight nuances to previously published versions of the theory, notably concerning the constitutive description of the subglacial water film and its flow.

A new numerical method is devised to solve the model, and we show that it can be solved for realistic values of most of the parameters, with the exception of that corresponding to the water film thickness. We show that evolved bedforms can be three-dimensional and of the correct sizes, and we explore to some extent the variation of the solutions with the model's parameters.

*Keywords:* Drumlins, ribbed moraine, mega-scale glacial lineations, instability.

## 1 Introduction

Drumlins are small ovoid hills which are formed under ice sheets. They occur in swarms, and are somewhat analogous to aeolian dunes or water waves, and equivalently may be thought of as occurring as the result of an instability of a state of uniform flow (Patterson and Hooke 1995, Pelletier 2008, Clark 2010, Hooke and Medford 2013), although this view is by no means universally accepted (Fisher and Shaw 1992, Hättestrand and Kleman 1999, Kleman and Hättestrand 1999, Lindén *et al.* 2008, Möller 2006, Möller 2010, Shaw 1983, Shaw 1994, Shaw and Kvill 1984, Shaw and Sharpe 1987, Shaw and Rains 1989). After the retreat of the ice sheets following the last ice age, much of the former subglacial topography has been exposed, revealing the widespread presence of drumlins (e.g., Clark *et al.* 2009); see figure 1 for an example.



Figure 1: A view from Westport harbour, Co. Mayo, Ireland, of some of the drumlins of Clew Bay.

Historical studies of drumlins date back more than 200 years (Hall 1815, Bryce 1833, Kinahan and Close 1872, Tarr 1894, Millis 1911, Gravenor 1953), and more recent significant developments are due to Smalley and Unwin (1968), Boulton (1987) and Menzies (1979a, 1979b). Much of the literature concerns the issue of whether drumlins are ‘erosional’ or ‘depositional’, ignoring the problem of describing how the topography of drumlinised terrain actually arises, despite this being its most obvious feature (Clark 2010).

Drumlins may be a part of a family of subglacial bedforms which includes ribbed moraine and glacial lineations (including MSGL — mega-scale glacial lineations), and it is possible that they are all formed by a similar mechanism, with the differences being due to different ice flow conditions (Ely *et al.* 2016, Sugden and John 1976), and indeed this appears consistent with the instability theory (Fowler and Chapwanya 2014), which is one of several theories (Pelletier 2008, Hooke and Medford 2013, Iverson *et al.* 2017) which has a viable quantitative (as opposed to descriptive) basis.

The instability theory in its most recent form treats the coupled subglacial flow of ice, water and sediment in the vicinity of the bed of an ice sheet. From its earliest statement by Hindmarsh (1998) and Fowler (2000), this theory has been developed in a sequence of papers (Dunlop *et al.* 2008, Fowler 2009, 2010a, 2010b, Fowler and Chapwanya 2014, Kyrke-Smith and Fowler 2014), and has now reached a reasonable state of maturity, which we develop a little further in this paper. It has been used to predict the formation of ribbed moraine (Chapwanya *et al.* 2011), as well as to

explain the various forms of internal architecture which have been observed (Stokes *et al.* 2013).

However, the development of this theory to a state where computations can reveal the full development of the sub-glacial landscape is hindered by its complexity. It is very difficult technically to construct a numerical method to solve the problem, although some efforts have been moderately successful (Fowler 2009, Chapwanya *et al.* 2011). Since the introduction of a dynamic description of water flow to the theory (Fowler 2010a,b), however, no such computational method has yet proved viable.

The theory of sub-glacial geomorphology shares this shortcoming with its sub-aerial counterpart, where the classic theory of landscape development (Smith and Bretherton 1972), formulated as a set of partial differential equations, led to hybrid numerical methods (Willgoose *et al.* 1991), which were eventually abandoned in favour of lattice-based models (Kramer and Marder 1992, Tucker and Slingerland 1994). These are successful in a kind of fashion, but they retain a philosophical element of curve-fitting, and need to be treated with caution.

Very recently, Barchyn *et al.* (2016) have applied the same idea to subglacial bedforms, concluding in particular that the range of observed bedforms (ribs, drumlins, MSGS) can all be produced from the same model by adjustment of parameters. Having said that, their model mechanisms are subject to criticism, insofar as they do not appear to reflect the physically appropriate processes involving water and sediment transport.

Our purpose in this paper is to develop a numerical method to solve the instability model in its most recent mature form. We therefore begin by recapping the present state of this theory, providing at the same time a gloss on some inaccuracies that remained in the version of Fowler and Chapwanya (2014).

## 2 The instability theory

The instability theory has been developed from its initial formulation over a number of years. The most recent incarnation is by Fowler and Chapwanya (2014), to which further explanatory reference may be made. Because of the development of this theory over a period of almost twenty years, it will be difficult to grasp for the reader new to the subject. We therefore begin by providing a synopsis of the theory. Table 1 provides a listing of the principal variables of the model, and table 2 lists the physical parameters. Other derived quantities are given in tables 3 and 4.

There are three constituent parts to the formulation of the theory, and we treat these in turn.

### 2.1 Ice flow

Ice is assumed to flow as a viscous fluid with constant viscosity over a deformable substrate (water-saturated till), on which it exerts a dimensional basal shear stress  $\tau_b$  which generates a sliding velocity through a sliding law which also depends on the effective normal stress  $N$  at the ice/till interface. The elevation of the till surface is



Symbol	Meaning
$A$	deformable till thickness
$b$	sediment surface
$B$	bedload transport function
$f(\bar{u}, N)$	dimensionless basal stress (sliding law)
$F$	basal stress perturbation
$h$	water film thickness
$J(\hat{J})$	convolution ice flow function (transform), (2.10).
$\mathbf{k}$	wave vector
$L(\hat{L})$	convolution ice flow function (transform), (2.10).
$N$	effective pressure
$q$	groundwater flux
$s$	basal ice surface
$\bar{u}$	dimensionless ice velocity
$w$	vertical ice velocity
$W$	basal water source (from till)
$\Gamma$	basal water source
$\Pi$	till effective pressure
$\tau_b$	basal shear stress
$\tau_e$	effective bed stress
$\Phi$	ice normal stress

Table 1: The principal variables of the model and their meaning. The parameters of the model are listed in table 2. Listings of the dimensional scales and dimensionless parameters are provided in tables 3 and 4.

$b$ , the elevation of the basal ice surface is  $s \geq b$ , and the intervening space is occupied by water, either in the form of a clast-filled water film (Creyts and Schoof 2009), or as stream or cavity flow. The situation is illustrated in figure 2.

There are a number of length scales in the problem which are used to non-dimensionalise the model. These are the ice sheet depth  $d_i$ , the drumlin elevation scale  $d_D$  (which is used to scale both  $s$  and  $b$ ), the till deformation scale  $d_T$  and the drumlin length scale  $l$ , and the latter are given by

$$d_D = \frac{\tau_b}{\Delta\rho_{wi}g}, \quad d_T = \frac{\tau_b}{\Delta\rho_{sw}g(1-\phi)}, \quad l = \left( \frac{\eta_i u_0 d_D}{\tau_b} \right)^{1/2} = \left( \frac{\eta_i u_0}{\Delta\rho_{wi}g} \right)^{1/2}, \quad (2.1)$$

where  $u_0$  is the velocity scale, defined below. The density differences are defined by

$$\Delta\rho_{wi} = \rho_w - \rho_i, \quad \Delta\rho_{sw} = \rho_s - \rho_w, \quad (2.2)$$

with  $\rho_{s,w,i}$  being the sediment particle/water/ice density. Two important dimensionless parameters are the aspect ratio  $\nu$  and corrugation parameter  $\sigma$ , and these are defined by

$$\nu = \frac{d_D}{l}, \quad \sigma = \frac{l}{d_i}. \quad (2.3)$$

Symbol	Meaning
$d_i$	ice sheet depth
$D_s$	sediment grain size
$g$	gravitational acceleration
$k$	till permeability
$l_i$	ice sheet extent (scale)
$l_c^*$	critical clast spacing
$q_b$	bedload transport scale
$u_0$	ice velocity
$\Delta\rho_{sw}$	$\rho_s - \rho_w$
$\Delta\rho_{wi}$	$\rho_w - \rho_i$
$\eta_i$	ice viscosity
$\eta_s$	till viscosity
$\eta_w$	water viscosity
$\rho_i$	ice density
$\rho_w$	water density
$\phi$	sediment porosity
$\psi$	hydraulic head

Table 2: The principal parameters of the model and their meaning.

There is a uniform state which is a simple shear flow over a flat bed with uniform till thickness; the sliding velocity in this uniform state is  $u_0$ , which is the velocity scale used in (2.1). For small undulations ( $\nu \ll 1$ ) in the ice/till interface (as we observe), the ice velocity is only weakly perturbed, and as a result the ice flow problem becomes an entirely linear one which can be solved by Fourier transform.

When this is done, we find that the (dimensionless) kinematic boundary condition for the ice (also known as the closure condition) is

$$w = \alpha s_t + \bar{u} s_x, \tag{2.4}$$

where

$$\alpha = \frac{d_T}{d_D} \equiv \frac{\Delta\rho_{wi}}{\Delta\rho_{sw}(1 - \phi)}, \tag{2.5}$$

and additionally  $\bar{u}$  (the dimensionless sliding velocity) is defined by

$$\overline{f(\bar{u}, N)} = 1; \tag{2.6}$$

here  $f(\bar{u}, N)$  is the dimensionless basal stress at the ice/till interface, the overline denotes a spatial average (so  $\bar{u}$  is a function of time only), and this condition represents a balance between the drag at the bed and the basal stress due to the overlying ice flow.

The normal velocity  $w$  in (2.4) is given by

$$w = J * \Phi + L * F, \tag{2.7}$$

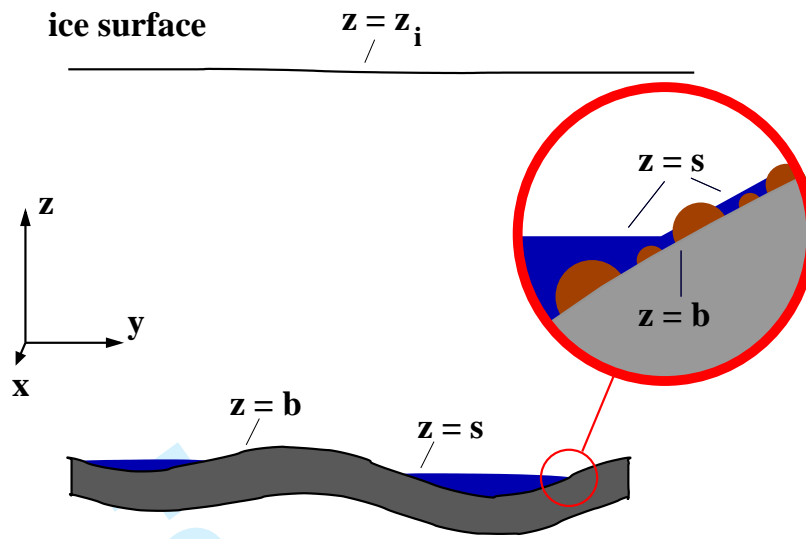


Figure 2: Illustration of the geometry of the problem.

where  $*$  denotes the Fourier convolution,

$$F = f(\bar{u}, N) - 1, \quad (2.8)$$

$F$  is the basal stress perturbation,  $\Phi$  is the ice normal stress, and the Fourier transform of a function is defined by

$$\hat{f}(\mathbf{k}) = \int_{-\infty}^{\infty} \int_{-\infty}^{\infty} f(x, y) e^{ik_1 x} e^{ik_2 y} dx dy, \quad (2.9)$$

where  $\mathbf{k} = (k_1, k_2)$ , and

$$\hat{J} = \frac{\sinh^2 j}{2k(j + \cosh j \sinh j)}, \quad \hat{L} = \frac{ik_1 j}{2k^2(j + \cosh j \sinh j)}, \quad j = \frac{k}{\sigma}. \quad (2.10)$$

Note that  $\hat{J}$  is bounded at  $k = 0$ , specifically

$$\hat{J}(0) = \frac{1}{4\sigma}. \quad (2.11)$$

The term in  $L$  is ignored, on the basis that it is small when  $j$  is large.

## 2.2 Water flow

We discuss water flow in greater detail than ice flow, because our previous theory is elaborated. Slow water flow through a thin film or stream of depth  $h$  is given by a local Poiseuille flow, and takes the dimensional form

$$h_t = \nabla \cdot \left[ \frac{h^3}{12\eta_w} \nabla \psi \right] + \Gamma + W, \quad (2.12)$$

where  $\psi$  is the hydraulic head,  $\eta_w$  is water viscosity, and  $\Gamma$  is the local water source due to internal melting in the ice.

The term  $W$  represents the net source of water to the film from the underlying saturated till, and is a new development in the theory. The reason for this flux is that if a cavity forms ( $h$  becomes large), then water to fill it must be sucked from the till, which will cause a decrease of  $b$ , compaction, and an increase in  $N$ . Fowler (2009) assumed that forming cavities would be rapidly infilled by upwards squeezing of the sediment, but did not concern himself with the consequence for water flow (which was only superficially described in that version of the theory). We now remedy that shortcoming.

We suppose that changes in  $b$  cause a primarily vertical flux of groundwater in the till, described by the conservation law

$$\phi_t + q_z = 0, \quad (2.13)$$

where  $\phi(\Pi)$  is the porosity of the till, which is a decreasing function of the effective pressure  $\Pi$  within the till, and the Darcy flux  $q$  is given by

$$q = \frac{k}{\eta_w} \left\{ \frac{\partial \Pi}{\partial z} + \Delta \rho_{sw} g (1 - \phi) \right\}. \quad (2.14)$$

The boundary conditions for the flow are

$$\begin{aligned} q &= 0 \quad \text{at} \quad z = 0, \\ \Pi &= N \quad \text{at} \quad z = b. \end{aligned} \quad (2.15)$$

If we suppose that  $\phi'$  (the prime denotes the derivative with respect to  $\Pi$ ) is sufficiently small that the flow response time is small (Fowler 2010a), then the water pressure is approximately hydrostatic,  $q$  is small, and if  $\phi$  does not vary too much,

$$\Pi \approx N + \Delta \rho_{sw} g (1 - \phi) (b - z). \quad (2.16)$$

Of interest is the water flux from the till to the film above. To calculate this, we integrate (2.13) from 0 to  $b$ . Using (2.16), we find

$$q_b \equiv q|_{z=b} \approx |\phi'| b \Pi_t = |\phi'| b \{N_t + \Delta \rho_{sw} g (1 - \phi) b_t\}. \quad (2.17)$$

Now exact integration of (2.13) from 0 to  $b$  shows that the net flux  $W$  from the till to the water film is

$$W = -\frac{d}{dt} \int_0^b \phi dz = q_b - \phi|_b b_t, \quad (2.18)$$

and thus

$$W = |\phi'| b N_t - \{\phi - |\phi'| \Delta \rho_{sw} g (1 - \phi) b\} b_t. \quad (2.19)$$

As a simple approximation, we will take

$$W \approx -\phi b_t. \quad (2.20)$$

We scale the equation (2.12) using the drumlin time scale

$$t_D = \frac{d_D l}{d_T u_0} \equiv \frac{\Delta \rho_{sw} (1 - \phi) l}{\Delta \rho_{wi} u_0}, \quad (2.21)$$

and in addition

$$\psi \sim \tau_b, \quad h \sim h_0, \quad W \sim \frac{\phi d_D}{t_D} = \frac{\phi d_T u_0}{l}, \quad (2.22)$$

and this leads us to the dimensionless form

$$\varepsilon \omega h_t = \nabla \cdot [h^3 \nabla \psi] + \omega - \Omega b_t, \quad (2.23)$$

in which the dimensionless hydraulic head is

$$\psi = -\sigma x + s - N + \Phi. \quad (2.24)$$

The definitions of the parameters assume a mean film thickness<sup>1</sup>

$$h_0 = \left( \frac{12 \eta_w l_i l \Gamma}{\tau_b} \right)^{1/3}, \quad (2.25)$$

where  $l_i$  is horizontal ice sheet scale, and then

$$\varepsilon = \frac{h_0}{\Gamma t_D}, \quad \omega = \frac{l}{l_i}, \quad \Omega = \frac{\phi d_T u_0}{\Gamma l_i}. \quad (2.26)$$

While this gives a way to accommodate suction of water from, or expulsion to, the underlying sediment, we shall later find that  $\Omega \ll 1$  so that in practice it is unimportant.

## 2.3 Sediment flow

Sediment flow is described by the Exner equation, which takes the dimensionless form

$$b_t + \bar{u} A_x = \beta \nabla \cdot [A^3 \nabla N] - \gamma \nabla \cdot [B(\tau_e) \tau_e], \quad (2.27)$$

where the dimensionless parameters are defined by Fowler and Chapwanya (2014):

$$\beta = \frac{2 d_T^2 \tau_b}{3 \eta_s l u_0}, \quad \gamma = \frac{q_b}{d_T u_0}, \quad (2.28)$$

where  $\eta_s$  is an assumed sediment viscosity and  $q_b$  is a bedload transport scale. These quantities are discussed further below. The choice of time scale in (2.27) was given in (2.21).

The fluxes comprise three terms. The first,  $\bar{u} A \mathbf{i}$ , represents the advection of till by the ice flow. The assumption is that the ice grips the till and drags it along as

<sup>1</sup>Note that (2.32) of Fowler and Chapwanya (2014) contains an error, corrected here, although the inferred value of  $h_0$  in table 2 of that paper is correct.



a shear flow. The quantity  $A$  is the dimensionless deformable till thickness, which is a function of the overlying shear stress  $\tau$  and the effective pressure at the ice/till interface  $N$ :

$$A = \frac{1}{2} \left[ \frac{\tau}{\mu} - N \right]_+, \quad \tau = f(\bar{u}, N). \quad (2.29)$$

It is a unimodal (one-humped) function of  $N$  since it is determined by the yield stress of the till which allows deformation. As  $N$  increases, the till becomes stiffer, which reduces  $A$ , but this is offset at small  $N$  by the fact that the driving stress itself increases with  $N$ . It is the fact that  $A$  increases with  $N$  at small  $N$  that enables the ribbing part of the instability to occur.

The first term on the right hand side of (2.27) is the till squeezing term. It indicates that till will be squeezed down effective pressure gradients, in keeping with Terzaghi's principle that the deformation of saturated granular materials (soils) is determined by the effective pressure. It is a stabilising term. The parameter  $\beta$  involves an assumed till viscosity. As a granular material, till has a yield stress, but this does not help in choosing a rheology, and a viscous flow law (with viscosity being such as to remain on the yield surface) is a straightforward choice, although the reality of the matter is doubtless more complicated. Since we can expect  $\tau_b \sim \frac{\eta_s u_0}{d_T}$ , we see that

$$\beta \sim \frac{d_T}{l}, \quad (2.30)$$

and is small.

The second term on the right of (2.27) represents bedload transport of sediment by stream flow.  $\tau_e$  is the effective bed stress due to water flow which drives the transport, and is given dimensionlessly by

$$\tau_e = -h \nabla \psi - \theta \nabla b, \quad (2.31)$$

where

$$\theta = \frac{2\Delta\rho_{sw}D_s}{\Delta\rho_{wi}h_0}; \quad (2.32)$$

here  $D_s$  is the sediment grain size. The bedload transport function  $B$  is an increasing function of  $\tau_e$ . A comment on this function is necessary. The normal scale of water film thickness is of the order of millimetres, and the flow is so slow that only the smallest particles might be moved; therefore it seems inappropriate to use a stream-based recipe as we do. On the other hand, we know that sub-glacial streams do occur, and indeed that floods occur between subglacial lakes, and from subglacial lakes to the ice sheet margin (e.g., Goodwin 1988, Engelhardt and Kamb 2013, Sergienko and Hulbe 2011), so some mechanism to form streams must exist. Given this, we associate the transport by bedload with the irregular occasions when a viable stream system exists. However, we do not expect such transport to occur all the time, but rather during occasional flood events (as indeed happens sub-aerially). This makes the choice of the bedload transport coefficient and the function  $B$  somewhat speculative. A typical stream flow choice is a power law  $B = \tau_e^{m-1}$ , where commonly  $m = \frac{3}{2}$ ,

but in the present situation, this function should be based on flood frequency and magnitude, which are not simply related to the mean water film thickness. Similarly,  $\gamma$  in (2.28) represents the ratio of mean water-borne sediment transport to till flux, and this also is very unconstrained. We estimate it as being small, but it is liable to be quite variable. Indeed, one can imagine situations where till is very stiff, so that most transport is water-borne, and in this case  $\gamma$  would be large. In our simulations, we use a value  $m = 3.5$  (partly because we require  $m > 3$  for the lineation instability).

The geometric relation between the ice base and sediment floor is

$$b = s - \delta h, \quad (2.33)$$

where

$$\delta = \frac{h_0}{d_D}, \quad (2.34)$$

and is present because the ice roof elevation and sediment floor elevation have a different scale ( $d_D$ ) to that of the water film depth ( $h_0$ ).

## 2.4 Ice ‘closure’

Counting equations, we see that (2.4), (2.6), (2.7), (2.8), (2.10), (2.23), (2.24), (2.27), (2.29), (2.31) and (2.33) provide twelve equations for the thirteen unknowns  $w$ ,  $s$ ,  $\bar{u}$ ,  $N$ ,  $J$ ,  $L$ ,  $\Phi$ ,  $F$ ,  $h$ ,  $\psi$ ,  $b$ ,  $A$  and  $\tau_e$ . An extra equation is necessary to close the system. In the classical stability theory (Hindmarsh 1998, Fowler 2000), this is taken to be the condition of constant hydraulic potential,  $\psi = -N_c$ , but in the present context, that is not enough, because we have explicitly introduced the water layer thickness  $h$ . Fowler (2009) accommodated  $h > 0$  (the formation of cavities) with the extra statement:

$$\begin{aligned} h &= 0 & \text{if } N > 0; \\ N &= 0 & \text{if } h > 0, \end{aligned} \quad (2.35)$$

and required nothing else. Fowler and Chapwanya (2014) modified this by including a closure equation of the form

$$\frac{\partial h}{\partial t} = \frac{\rho_w \Gamma}{\rho_i} - \frac{l_c^* N}{\eta_i N^*(h)}, \quad (2.36)$$

where  $\Gamma$  is the basal melting rate,  $l_c^*$  is a critical ‘clast spacing’ length scale of the rough till surface, and  $N^*(h)$  is a sharply decreasing function of  $h$ . In equilibrium, (2.36) provides a continuous approximation to (2.35), but its provenance is suspect, despite its resemblance to the classic Röthlisberger closure equation.

To see this, we recall that the Röthlisberger theory (Röthlisberger 1972, Nye 1976) consists of equations representing conservation of mass, momentum and energy for water flow in a semi-circular conduit, which provide three equations for the four variables  $Q$  (volume flux),  $S$  (cross-sectional area),  $m$  (melting rate) and  $N$  (effective pressure), and the theory is completed by a closure equation. This apparently provides

a second evolution equation for  $S$ , which makes the theory seem strange. In fact, this closure equation is determined by the viscous closure of the ice, and is actually a representation of the kinematic boundary condition of the ice flow.

Given this, our cause for concern in specifying (2.36) is that it presumably also represents a kinematic boundary condition for the ice flow; but we have already prescribed this in writing (2.4)! Although the two equations clearly represent processes at two different length scales, it is not clear how a single kinematic equation should be able to give rise to *two* equations. We therefore re-examine this issue.

We now take an alternative view. The till is a compressible porous medium with a porosity  $\phi$  which, in the normal way of soil mechanics, is taken to be a decreasing function of the effective pressure in the till,  $\phi = \phi(\Pi)$ . In our discussion of the water film, we conceive of it as a discrete layer *lying within the upper surface of the till*. It is in fact a second porous layer of very small thickness. As such, its porosity  $\phi_s$  can be taken to be a function of its effective pressure  $N$ . Further, it seems clear that the effective porosity of the surface should be an increasing function of the film thickness. The consequence of all this is that we may take layer thickness to be a decreasing function of  $N$ ,

$$h = G(N), \quad (2.37)$$

which mimics (2.36) but lacks the time derivative. Since in our earlier work (Fowler and Chapwanya 2014) this time derivative term was small, our stability results there remain valid.

In specifying a suitable form for  $G(N)$ , we introduce a *critical clast size*  $h_c$ , which is a measure of the coarseness of the till. Our concept of the water film is that of Creyts and Schoof (2009), embedded as a water layer within the topmost clasts of the till, such that when its thickness exceeds  $h_c$ , then the ice loses its grip on the till and the effective pressure becomes zero. In reality, it is more likely that  $h_c$  represents the length scale over which  $N$  approaches zero.

As  $h \rightarrow 0$ , we suppose that the effective pressure should approach  $N_0$ , which would be the effective pressure necessary to evacuate the water flux entirely through the till. Any reasonable calculation suggests that this is very high. For example, evacuation of a vertical flux of  $3 \text{ mm y}^{-1}$  to a canal at distance  $10 \text{ km}$  through a substrate of permeability  $10^{-15} \text{ m}^2$  requires an effective pressure of  $\sim 10^6 \text{ Pa}$ , calculated using Darcy's law: not unreasonable, but enormous in terms of typical effective pressures necessary to deform till.

If  $N$  changes by  $O(N_0)$  when  $h$  changes by  $O(h_c)$ , then in dimensionless terms

$$-\frac{\partial N}{\partial h} \sim \frac{1}{\lambda}, \quad \lambda = \frac{\tau_b h_c}{N_0 h_0}, \quad (2.38)$$

since  $N$  is scaled with  $\tau_b$  and  $h$  with  $h_0$ . In the absence of any further information, we take

$$\lambda h N = 1 \quad (2.39)$$

as a credible dimensionless candidate for this water film law. While this is mathematically more or less identical to the formulation of Fowler and Chapwanya (2014), the physical description is quite different, and the definition of the corresponding parameter to  $\lambda$  (which was there denoted as  $\Pi$ ), is quite different.

Symbol	Meaning	Typical value
$d_D$	drumlin elevation	11 m
$d_T$	till deformation depth	1 m
$h_0$	water film thickness	6 mm
$l$	drumlin length	640 m
$l_i$	ice sheet horizontal length scale	$10^3$ km
$h_c$	critical clast size	0.1 m
$N_0$	film-free effective pressure	$10^6$ Pa
$t_D$	time scale	74 y
$\Gamma$	melt rate	$3 \text{ mm y}^{-1}$
$\tau_b$	basal shear stress	$0.9 \times 10^4$ Pa

Table 3: Derived values of scales.

Symbol	Typical value	Interpretation
$\alpha$	0.09	Ice flow time scale
$\beta$	$1.04 \times 10^{-3}$	Till squeezing
$\gamma$	$0.3 \times 10^{-2}$	Stream bedload
$\delta$	$0.54 \times 10^{-3}$	Water film thickness
$\varepsilon$	$2.7 \times 10^{-2}$	Film flow time scale
$\theta$	0.62	Downslope component of stream stress
$\lambda$	0.15	Variation of film thickness with effective pressure
$\mu$	0.6	Granular friction coefficient
$\nu$	$1.7 \times 10^{-2}$	drumlin roughness (aspect ratio)
$\sigma$	0.64	drumlin corrugation (length/ice depth)
$\omega$	$0.41 \times 10^{-6}$	meltwater source
$\Omega$	0.01	pore water suction from till

Table 4: Approximate dimensionless parameter values. The ‘interpretation’ means that the parameter can be thought of as a measure of the size of the indicated quantity.

## 2.5 A reduced model

Values of the constants used in scaling, and the values of the resulting dimensionless parameters were estimated by Fowler and Chapwanya (2014), and are summarised in tables 3 and table 4. Many of the parameters are small, and we neglect some but retain others, as discussed below. A particular point concerns the magnitude and form of the water-borne sediment transport term. As mentioned following (2.32), this term uses standard assessments of bedload transport to estimate  $\gamma$ , but in fact the term can only have useful meaning during flood events or in localised stream flow, so the effective magnitude of  $\gamma$  and the form of the transport function  $B(\tau_e)$  are not well constrained.

Although the model is complicated, its structure is relatively simple, as we now explain. The principal describing equations are the Exner equation (2.27) for  $b$ , the

water mass equation (2.23) for  $\psi = -\sigma x + \Psi$ , and the ice flow kinematic condition (2.4) for  $s$ :

$$\begin{aligned} b_t + \bar{u}A_x &= \beta \nabla \cdot [A^3 \nabla N] - \gamma \nabla \cdot [B(\tau_e) \tau_e], \\ \nabla \cdot [h^3 \nabla \Psi] &= \sigma (h^3)_x, \\ \alpha s_t + \bar{u}s_x &= J * \Phi, \end{aligned} \quad (2.40)$$

in which we suppose  $J$  is given by the inverse of  $\hat{J}$  in (2.10). We have ignored the small terms in  $\omega$  and  $\Omega$ , but not those in  $\beta$  and  $\gamma$  in (2.40)<sub>1</sub>. The term in  $\beta$  is a necessary stabilising term, and will actually increase in magnitude as  $N \rightarrow 0$ , since the till becomes much more fluid then (although this is offset by the decrease in  $A$ ). The term in  $\gamma$  allows the ribbing instability associated with the formation of lineations via the production of stream flow. Thus both of these terms are essential.

These equations for  $b$  and  $\psi$  introduce five subsidiary variables,  $A$ ,  $N$ ,  $\tau_e$ ,  $\Phi$  and  $h$ . These are determined by the equations

$$\begin{aligned} \Psi &= s - N + \Phi, \\ A &= \frac{1}{2} \left[ \frac{f(\bar{u}, N)}{\mu} - N \right]_+, \\ \lambda h N &= 1, \\ b &= s - \delta h, \\ \tau_e &= -h[\nabla \Psi - \sigma \mathbf{i}]. \end{aligned} \quad (2.41)$$

We have neglected the term in  $\theta$  on the basis that  $\gamma\theta$  is small; the term in  $L$  in (2.7) on the basis that  $\sigma$  is relatively small (thus  $j$  large); but we do not neglect  $\delta$  because the term  $\delta h$  is singular; we actually use (2.41)<sub>4</sub> to determine  $h$ .

## 2.6 Instability mechanisms

We now recall the instability mechanisms in the model (Fowler and Chapwanya 2014). The ribbing instability is due to the advective term in (2.40)<sub>1</sub>, when  $A'(N) > 0$ ; the mechanism is somewhat analogous to mechanisms of (transverse) dune formation, insofar as the maximum sediment transport is shifted upstream of the bed elevation maximum.

In more detail, Smith (1970) and Engelund (1970) were the first to show that the formation of aeolian or fluvial dunes due to the action of wind or water flow could be ascribed to the fact that the forming dunes altered the overlying (turbulent) fluid flow in such a way as to shift the maximum of the shear stress at the bed *upstream* of the maximum dune elevation; this was achieved by solving the approximating Orr–Sommerfeld equation for the disturbance to the flow. In consequence, the maximum sand transport is also shifted upstream, and a simple consideration of the Exner equation explains the resulting instability.

In the present theory, the predominant transport of sediment is also presumed to be by its shear by the overlying ice, and the instability is also due to this transport



being maximal upstream of the bed elevation maximum, due to an increase in the bed shear stress because of a presumed dependence of the sliding law on the effective pressure. It is not, however, an increase in the ice flow velocity which increases the till flux, but an increase of the deforming till depth (i.e., the depth to the critical yield stress where  $N = \tau_b/\mu$ ). The instability mechanism is the same as that for dune formation, but for a somewhat different reason.

The lineation instability is due to the term in  $\gamma$  in  $(2.40)_1$ , and is analogous to the rilling instability of Smith and Bretherton (1972); in the present case, it requires the bedload function  $B$  to be sufficiently rapidly increasing: if we assume a power law  $B \propto \tau_e^{m-1}$ , then we require  $m > 3$ . In Smith and Bretherton's theory, regularisation of the instability at high wave number is provided by the small term in  $\delta$  in  $(2.41)_4$  (Loewenherz 1991, Loewenherz-Lawrence 1994, Fowler *et al.* 2007).

Physically, one can interpret this part of the instability mechanism as occurring because the formation of transverse ribs causes a pooling of water in the troughs, and one naturally expects such forming pools to be unstable and lead to downstream water flow. The distinction between the 'drumlin' and 'lineation' features that we exhibit below is essentially one of the amount of water and the efficiency with which it can transport sediment.

The term in  $\beta$  is stabilising; thus all three derivative terms in  $(2.40)_1$  are important to retain. In addition the nonlinear coefficient  $h^3$  features importantly in the stability analysis, particularly for lineations, but the coefficient  $h$  in  $\tau_e$  seems less significant.

### 3 Numerical solution

We aim to solve  $(2.40)$  and  $(2.41)$ , assuming periodic boundary conditions on the boundaries of our square domain, which seems appropriate, given that this area represents a small segment of a much larger bedform field. The function  $A(N)$  is described by Fowler (2009), and we have followed its approximation as given by Fowler (2009) and Chapwanya *et al.* (2011). Efforts to solve such equations have previously used an entirely spectral approach (Fowler 2009, Chapwanya *et al.* 2011), mainly because the convolution term in  $(2.40)_3$  is most easily dealt with this way. This causes technical difficulties, however, because rapid changes in  $N$  cause the generation of high wave number components, and the requirement for  $N$  to remain positive provides a serious constraint on numerical implementation. Efforts to implement such a method for the version of the model given by Fowler and Chapwanya (2014) failed entirely, however.

Here we provide a different numerical method which appears to be relatively successful. It is based on time-stepping the equations for  $b$  and  $s$ ,  $(2.40)_1$  and  $(2.40)_3$ ; we use finite differences to compute the spatial derivatives in the  $b$  equation, but a spectral method for the  $s$  equation. Both equations are integrated forward using the method of lines.

Having stepped  $s$  and  $b$  forward,  $(2.41)_4$  determines  $h$ ,  $(2.41)_3$  then determines  $N$ ,  $(2.40)_2$  can be solved to determine  $\Psi$ , and then  $(2.41)_1$  gives  $\Phi$ . We can then proceed to the next time step. We assume periodic boundary conditions in both  $x$  and  $y$  directions for  $s$ ,  $b$  and  $\Psi$ .

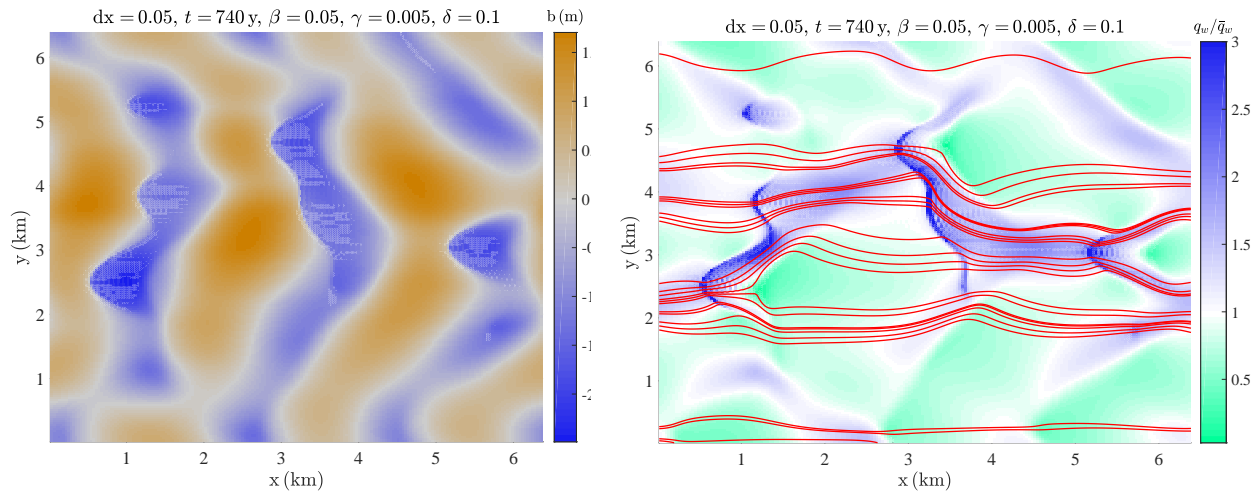


Figure 3: Rib-like features at  $t = 740$  y. Parameter values  $\delta = 0.1$ ,  $\gamma = 0.005$ ,  $\beta = 0.05$ . On the left is shown the topography, while on the right is shown the water flux (as a fraction of the mean); green areas are essentially dry, and the red curves are streamlines for water flow, spaced with equal amounts of water flux between them. Essentially the water makes its way over the topography, but there is evidence of streaming flow. The dimensionless box length and width is 10, and the dimensionless space step is 0.05, although the data are all plotted dimensionally.

For the initial conditions, we mostly assume small random perturbations about the base state  $b = 0$  and  $s = \delta$ ; typically these are of dimensionless magnitude  $\sim 10^{-3}$ , corresponding to elevation variations of a few centimetres.

In solving for  $\Psi$  in  $(2.40)_2$ , central differencing is used for the nonlinear Laplacian, and a backward difference for the advective term. This yields a linear inhomogeneous matrix equation for the components of  $\Psi$ , but the matrix is singular, due to the fact that with periodic boundary conditions, the solution of  $(2.40)_2$  can only be determined up to addition of an arbitrary constant. To resolve this degeneracy, note that by averaging  $(2.40)_3$  over the domain, we obtain

$$\alpha \bar{s}_t = \frac{\bar{\Psi} + \bar{N} - \bar{s}}{4\sigma}, \quad (3.1)$$

using periodicity of  $s$ ,  $(2.41)_1$ , and  $(2.11)$ . Additionally, we have  $\bar{b}_t = 0$ , whence we can take  $\bar{b}$  to be constant and equal to its initial value, and therefore  $(3.1)$  leads to

$$4\sigma\alpha\delta\bar{h}_t = \bar{\Psi} + \frac{\bar{h}^{-1}}{\lambda} - \delta\bar{h} - \bar{b}. \quad (3.2)$$

With periodic boundary conditions, there is no net water flow into the domain, and consequently  $\bar{h}_t = 0$ . This would actually be a consequence of integrating  $(2.23)$  over the domain, if we take the source term  $\omega = 0$ . However, it appears slightly worrying that if  $\omega \neq 0$ , then  $\varepsilon\bar{h}_t = 1$ . The issue is that the source is absorbed into an increase

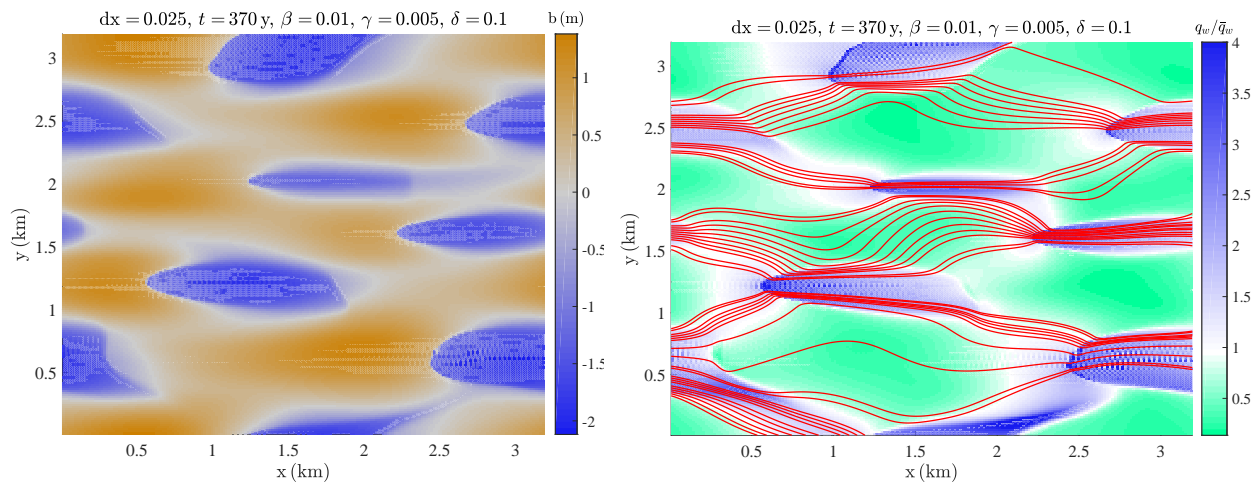


Figure 4: Drumlin-like features at  $t = 370$  y. Parameter values  $\delta = 0.1$ ,  $\gamma = 0.005$ ,  $\beta = 0.01$ . The water flow begins to be concentrated in stream segments and to flow round the bedforms (right), while the bedforms are somewhat drumlin-like.

of water flux through the domain, so that exact periodicity is not required. With this proviso, we take  $\bar{h}_t = 0$ , and thus

$$\bar{\Psi} = \bar{b} + \delta \bar{h} - \frac{\bar{h}^{-1}}{\lambda}. \quad (3.3)$$

In differencing the  $b$  equation, we use flux-conservative central differences for the diffusion terms, but for the two convective terms (the term in  $A_x$  and that for  $(Bh)_x$  in  $\nabla \cdot [B\tau_e]$ ), the expected sharp changes in  $N$  and thus  $h$  suggest upwinding, but it is not obvious in which direction this should be. To circumvent the issue, we have chosen to compute the first derivative terms spectrally, thus for example

$$A_x = \mathcal{F}^{-1}[-ik_1 \hat{A}], \quad (3.4)$$

where  $\mathcal{F}$  is the Fourier transform. While this appears to give good results, it does rely on the use of periodic boundary conditions, and on the splitting technique applied.

In solving the problem numerically, we have found that of the three critically small parameters  $\beta$ ,  $\gamma$  and  $\delta$ , the first two can be reduced satisfactorily without undue numerical issues, but the value of  $\delta$  causes serious problems, as the solutions become increasingly singular, and we have not been able to obtain useful results for values of  $\delta < 0.1$ ; obviously this is a shortcoming of our method. More specifically, sharp changes in  $h$  occur, and as found by Fowler (2009) and Chapwanya *et al.* (2011), the spectral parts of the code cause Gibbs-like phenomena to occur. Unlike the latter paper, we have not resorted to filtering of high wave number components.

In the electronic supplementary material, we provide three fairly typical movies of the solutions through time with different choices of parameter values. In figures 3, 4 and 5, we show the final frame of these runs. During the course of the evolution of the bedforms with time, they typically are rib-like at early times, and they continue

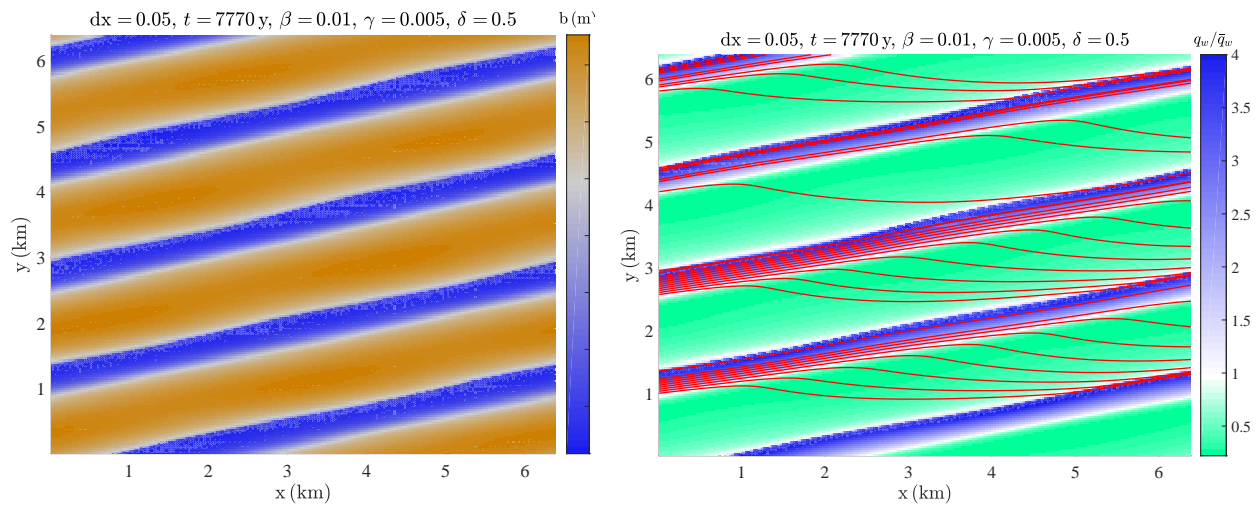


Figure 5: Lineation-like features at  $t = 7,770$  y. Parameter values  $\delta = 0.5$ ,  $\gamma = 0.005$ ,  $\beta = 0.01$ . The water flow is concentrated into streams between the lineations.

to evolve with time. Figure 3 shows bedforms which are somewhat rib-like, figure 4 shows three-dimensional structures analogous to drumlins, and figure 5 resembles lineations, though it should be pointed out that the ‘lineations’ are inclined to the direction of ice flow (in the  $x$  direction). Apart from the parameters in table 4, we use values  $\lambda = 1$  and  $m = 3.5$ .

The lineations in figure 5 are inclined to the ice flow because there is a net lateral water flux. Our use of periodic boundary conditions allows this, and it seems admissible in the model. We think this odd occurrence is due to the assumption of a pathologically flat initial surface. In reality, there is always some topographic variation, and we might suppose that any lateral valley-like topography will act to confine the water flow in a local catchment, but we have not been able provide a satisfactory numerical illustration of this.

In the figures (but not in the movies), we have included streamlines  $\chi = \text{constant}$  representing water flow, where

$$\chi = \int q_1 dy - q_2 dx, \quad \mathbf{q} = (q_1, q_2). \quad (3.5)$$

Some interpretation of these is necessary. Firstly, the streamlines are not periodic in  $x$ , nor need they be. For example, the streamlines of  $\chi = y - x$  are just a family of straight lines, but the velocity field is periodic.

Bunching of streamlines indicates streaming, and thus we see that in figure 3, water begins to be focussed in streams, while in the drumlin figure 4, water focusses in the depressions, which are in essence cavities, and flows round the elevations; finally in figure 5, stream flow is confined to the valleys between the lineations.

## 4 Discussion

### 4.1 The model

A model is, of course, only that. But within the attempt to describe the physical processes, there are a great many assumptions which are made. Some of these are more critical than others; we now offer a commentary on some of them. That ice viscosity is Newtonian seems unlikely to be critical. Similarly with the assumption of an effectively viscous till. What is critical for till deformation is that  $A(N)$  is a concave function of  $N$ , and this requires two things: no deformation below the yield stress, and a sliding law in which basal stress is an increasing function of  $N$ . While this is a common deduction in hard bed sliding laws, a precise derivation requires a presumption of till rheology, and such studies are not well advanced. On the other hand, the equivalent presumption that till becomes more deformable as effective pressure is reduced seems intuitively reasonable.

Of more concern is the way in which we model water flow. Firstly, the way in which the Creyts–Schoof water film is described by a relation between water depth and effective pressure is open to further scrutiny, and, more so than the sliding law, this ‘water film law’ is largely heuristic. This is important, because, as shown by Fowler and Chapwanya (2014), its parametric form is critical to the form of the resulting instability.

Water flow, and accompanying sediment transport, is modelled as a continuous process but this cannot be the actual case. In particular, sediment transport can only practically occur during floods, and does not occur continuously. While a continuous model nevertheless makes sense, it becomes unrealistic to model sediment transport using sub-aerial correlations. In particular, the size and frequency of floods will themselves depend on details of the water flow. For example, we might suspect that floods only occur for a sufficiently large water flux, and thus  $h$ . In this case we would effectively have  $B = 0$  for  $h$  less than some critical value, and increasing rapidly thereafter; in a power law  $B \propto \tau_e^m$ , this would correspond to a high value of  $m$ .

### 4.2 Computations

The principal limitation of the computations is the inability to reduce  $\delta$  to a sensibly small value. Small  $\delta$  causes sharp changes in  $h$ , which can only be resolved by taking inordinately small space step sizes, which makes computation time (which is already long) prohibitive. Certainly this is an issue for future study. It should be noted that the long times over which the bedforms evolve in the simulations is an artifact of the high values of  $\delta$  used. In reality, we expect that for smaller values, the time scales of bedform evolution will be nearer to decades.

### 4.3 Comparison with linear stability results

Naturally, one wants to compare the results with our earlier stability results (Fowler and Chapwanya 2014). Our results are indeed consistent, at least for the early growth



phase, but the nonlinear evolution deviates from this, so that a comparison is not so straightforward.

The linear stability analysis of Fowler and Chapwanya (2014) showed that variation of the parameter  $\Pi$  (from 0.7 to 10 in figure 4 of that paper) accounted for instability results corresponding to ribs, drumlins, and MSGSL. While the model presented in this paper is a slight variant of this previous work, the stability results are analogous. In our case, the parameter  $\lambda$  now plays the rôle of  $\Pi$ , with  $\lambda$  in the range 1–15 demonstrating the same qualitative transition from ribs to MSGSL (in terms of linear stability results). Note that these stability results assume fixed values for  $\beta$ ,  $\gamma$  and  $\delta$ , as in Fowler and Chapwanya (2014), and consistent with those in table 4.

Our approach in this paper has been orthogonal, as we have focussed on the ability to obtain credible numerical results. The parameters we have used have, for this reason, not been the same as those in table 4; in particular, the value of  $\delta$  used is much larger. For the three parameter combinations presented above, the linear stability analysis predicts the formation of ribs at early times, and indeed, this behaviour is seen in the movies in the supplementary material. Beyond this initial linear growth phase, however, the bedforms evolve nonlinearly, and the differing outcomes are due to the different nonlinear evolution at these different parameter values.

#### 4.4 Results

The three figures indicate that a variety of bedforms can be produced, both by varying the parameters, and also by looking at different times within one run. For example, the run which yields figure 5 shows drumlin-like behaviour at 4,000 years, and rib-like bedforms earlier on. Despite such large time scales being a consequence of the artificially large value of  $\delta$  used, the fact that bedforms may continue to evolve over time has an implication for any practical conclusions we might wish to make, because while we assume constant ice flow conditions in our simulations, it is likely that ice flow magnitude, basal shear stress and flow direction will all change in time, making the issue of prediction something of a free-for-all. While it is tempting to rush into such experiments, it may be advisable to await such time as confidence in the veracity of the model (not to mention the numerical computations) improves.

In the figures, we have plotted contours indicating stream flow, and it is noticeable that the flow becomes localised, consistent with the expectation of Kyrke-Smith and Fowler (2014). It is also found that the ‘streams’ remain of millimetric dimensions; large cavities do not form (or as they do, they are infilled (Fowler 2009)), and we suppose that the millimetric stream thickness represents a time average of occasional flood events.

One comment we might make concerning the movies is that the initial instability occurs at smaller wavelengths than the later evolved bedforms. This behaviour is similar to that found by Chapwanya *et al.* (2011), and is a common feature in many systems, particularly those involving granular flows (Meier *et al.* 2008), but our simulations do not indicate that the coarsening continues indefinitely.

## 4.5 Criticisms

We mentioned in the introduction that there are a number of other models in existence for bedform formation, although few of these are quantitatively based, but the promotion of other theories carries an implication that the instability theory may be unrealistic. We comment on two such criticisms.

Some time ago, Schoof (2007a,b) offered three objections to the instability theory, as it then existed. The first of these were that the instabilities were inherently two-dimensional, and could thus not explain drumlins. This led Dunlop *et al.* (2008) to adopt a defensive position where they restricted their aim to the explanation of ribbed moraine. More recent work (Fowler and Chapwanya 2014) indicates that this criticism is without foundation. Schoof also thought that the existence of internal stratification was inconsistent with the view of drumlins as travelling wave forms, but this view was rebutted by Stokes *et al.* (2013), who indicated that internal stratification would be maintained in a net erosional environment. Finally, Schoof suggested that the onset of cavitation would restrict drumlin amplitudes in the instability theory to a few metres, although it turns out such amplitudes are commonly observed (Spagnolo *et al.* 2012). Our present results, while not conclusive, are certainly consistent with this view, so this objection still has some merit.

A more recent challenge to the theory lies in the detailed observations of drumlins at Mulajökull by McCracken *et al.* (2016). These observations provide two results which, it is suggested, are inconsistent with the instability theory. The first is that till fabrics indicate till deformation by shear, which is supposed to be inconsistent with the instability theory assumption of compressive stresses. This objection appears to result from a misreading of the theory, which indeed yields instability via a negative flux divergence in the Exner equation (2.27), which can be written in the form

$$\begin{aligned} b_t &= -\nabla \cdot \mathbf{q}_b, \\ \mathbf{q}_b &= \bar{u}A\mathbf{i} - \beta A^3 \nabla N + \gamma B \boldsymbol{\tau}_e. \end{aligned} \quad (4.1)$$

The largest contribution is the ice-dragged till flux, which is indeed a shearing flow, and the negative divergence (upstream of a maximum bed elevation) arises not from a slow down of the till velocity but from a change in deformable till thickness,  $A$ , due to changes in  $N$ .

The second objection is that it is observed at Mulajökull (which is a surging glacier) that in the quiescent phase between surges, the effective pressure  $N$  is higher between the drumlins rather than lower, as the instability theory would suggest. This is indeed contradictory to the instability theory, but may be distracting because the surging appears to be fundamentally related to the process of drumlin growth. Indeed, it may be reasonable to suppose that surges are associated with a drainage switch between channels (with high  $N$ ) in the quiescent phase and a distributed system (with low  $N$ ) in the surge phase (Fowler 1987). The instability theory in the form presented here does not address what would happen if a glacier is of surge type, nor indeed does it have anything to say about drumlin formation under temperate glaciers with copious water flow. It would of course be of interest to adapt the theory

to confront the observations, but from a theoretical perspective, that is an extremely ambitious task. To be fair, however, Menzies (1979a) also makes a similar comment, so it may be that this criticism is more widely valid.

## 5 Conclusions

We have presented the current edition of the instability theory of drumlin formation, and we have provided a numerical method which is able to solve it, although not presently sufficiently near actual parameter values. As we vary the critical parameters  $\beta$ ,  $\gamma$  and  $\delta$ , we find that bedforms of the correct size and elevation develop, that the solutions may be time-dependent over sufficiently long time scales that external ice sheet time dependence will have an effect, and that snapshots of bedforms resembling ribbed moraine, drumlins and lineations are all obtainable. These results open the way to a comparison with actual observed bedforms, although such a comparison is presently premature.

### Data accessibility

The paper contains no data.

### Competing interests

We have no competing interests.

### Authors' contributions

A.C.F. devised the project, and wrote the paper. J.S.F. and I.R.M. constructed and solved the numerical model. All authors performed the literature review, and contributed to the analytic and numerical work. All authors worked on the final text.

### Acknowledgements

For continuing fruitful discussions, our thanks to Chris Clark, Chris Stokes, Jeremy Ely and Matteo Spagnolo.

### Funding statement

This publication has emanated from research conducted with the financial support of Science Foundation Ireland under grant numbers SFI/12/IA/1683 and SFI/13/IA/1923.

### Ethics statement

This research poses no ethical considerations.

## References

- Barchyn, T. E., T. P. F. Dowling, C. R. Stokes and C. H. Hugenholtz 2016 Subglacial bedform morphology controlled by ice speed and sediment volume. *Geophys. Res. Letts.* **43**, doi:10.1002/2016GL069558.
- Boulton, G. S. 1987 A theory of drumlin formation by subglacial sediment deformation. In: *Drumlin symposium*, eds. J. Menzies and J. Rose, Balkema, Rotterdam, pp. 25–80.
- Bryce, J. 1833 On the evidences of diluvial action in the north of Ireland. *J. Geol. Soc. Dubl.* **1**, 34–44.
- Chapwanya, M., C. D. Clark and A. C. Fowler 2011 Numerical computations of a theoretical model of ribbed moraine formation. *Earth Surf. Proc. Landf.* **36**, 1,105–1,112.
- Clark, C. D. 2010 Emergent drumlins and their clones: from till dilatancy to flow instabilities. *J. Glaciol.* **51**, 1,011–1,025.
- Clark, C. D., A. L. C. Hughes, S. L. Greenwood, M. Spagnolo, and F. S. L. Ng, 2009 Size and shape characteristics of drumlins, derived from a large sample, and associated scaling laws. *Quat. Sci. Revs.* **28**, 677–692.
- Creyts, T. T. and C. G. Schoof 2009 Drainage through subglacial water sheets. *J. Geophys. Res.* **114**, F04008, doi:10.1029/2008JF001215.
- Dunlop, P., C. D. Clark, and R. C. A. Hindmarsh 2008 Bed ribbing instability explanation: testing a numerical model of ribbed moraine formation arising from coupled flow of ice and subglacial sediment. *J. Geophys. Res.* **113**, F03005, doi:10.1029/2007JF000954.
- Ely, J. C., C. D. Clark, M. Spagnolo, C. R. Stokes, S. L. Greenwood, A. L. C. Hughes, P. Dunlop and D. Hess 2016 Do subglacial bedforms comprise a size and shape continuum? *Geomorphology* **257**, 108–119.
- Engelhardt, H. and B. Kamb 2013 Kamb Ice Stream flow history and surge potential. *Ann. Glaciol.* **54**, 287–298.
- Engelund, F. 1970 Instability of erodible beds. *J. Fluid Mech.* **42**, 225–244.
- Fisher, T. G. and J. Shaw 1992 A depositional model for Rogen moraine, with examples from the Avalon Peninsula, Newfoundland. *Can. J. Earth Sci.* **29**, 669–686.
- Fowler, A. C. 1987 A theory of glacier surges. *J. Geophys. Res.* **92**, 9,111–9,120.
- Fowler, A. C. 2000 An instability mechanism for drumlin formation. In: *Deformation of subglacial materials*, eds. A. Maltman, M. J. Hambrey and B. Hubbard, Spec. Pub. Geol. Soc. **176**, pp. 307–319. The Geological Society, London.

- Fowler, A. C. 2009 Instability modelling of drumlin formation incorporating lee-side cavity growth. *Proc. R. Soc. Lond. A* **465**, 2,681–2,702.
- Fowler, A. C. 2010a The instability theory of drumlin formation applied to Newtonian viscous ice of finite depth. *Proc. R. Soc. Lond. A* **466**, 2,673–2,694. doi: 10.1098/rspa.2010.0017.
- Fowler, A. C. 2010b The formation of subglacial streams and mega-scale glacial lineations. *Proc. R. Soc. Lond. A* **466**, 3,181–3,201. doi: 10.1098/rspa.2010.0009.
- Fowler, A. C. and M. Chapwanya 2014 An instability theory for the formation of ribbed moraine, drumlins and mega-scale glacial lineations. *Proc. R. Soc. Lond. A* **470**, 20140185.
- Fowler, A. C., N. Kopteva, and C. Oakley 2007 The formation of river channels. *SIAM J. Appl. Math.* **67**, 1016–1040.
- Goodwin, I. D. 1988 The nature and origin of a jökulhlaup near Casey Station, Antarctica. *J. Glaciol.* **34**, 95–101.
- Gravenor, C. P. 1953 The origin of drumlins. *Amer. J. Sci.* **251**, 674–681.
- Hall, J. 1815 On the revolutions of the Earth's surface. *Trans. Roy. Soc. Edinb.* **7**, 169–184.
- Hättestrand, C. and J. Kleman 1999 Ribbed moraine formation. *Quat. Sci. Revs.* **18**, 43–61.
- Hindmarsh, R. C. A. 1998 The stability of a viscous till sheet coupled with ice flow, considered at wavelengths less than the ice thickness. *J. Glaciol.* **44** (146), 285–292.
- Hooke, R. LeB. and A. Medford 2013 Are drumlins a product of a thermo-mechanical instability? *Quat. Res.* **79**, 458–464.
- Iverson, N. R., R. G. McCracken, L. K. Zoet, Í. Ö. Benediktsson, A. Schomacker, M. D. Johnson and J. Woodard 2017 A theoretical model of drumlin formation based on observations at Múlajökull, Iceland. *J. G. R. Earth Surface*, in press.
- Kinahan, G. H. and M. H. Close 1872 The general glaciation of Iar-Connaught and its neighbourhood, in the counties of Galway and Mayo. Hodges, Foster and Co., Dublin.
- Kleman, J. and C. Hättestrand 1999 Frozen-bed Fennoscandian and Laurentide ice sheets during the last glacial maximum. *Nature* **402**, 63–66.
- Kramer, S. and M. Marder 1992 Evolution of river networks. *Phys. Rev. Letts.* **68**, 205–208.



- Kyrke-Smith, T. M. and A. C. Fowler 2014 Subglacial swamps. *Proc. R. Soc. Lond. A* **470**, 20140340.
- Kyrke-Smith, T. M., R. F. Katz and A. C. Fowler 2014 Subglacial hydrology and the formation of ice streams. *Proc. R. Soc. Lond. A* **470**, 20130494.
- Lindén, M., P. Möller and L. Adrielson 2008 Ribbed moraine formed by subglacial folding, thrust stacking and lee-side cavity infill. *Boreas* **37**, 102–131.
- Loewenherz, D. S. 1991 Stability and the initiation of channelized surface drainage: a reassessment of the short wavelength limit. *J. Geophys. Res.* **96**, 8,453–8,464.
- Loewenherz-Lawrence, D. S. 1994 Hydrodynamic description for advective sediment transport processes and rill initiation. *Water Resour. Res.* **30**, 3,203–3,212.
- McCracken, R. G., N. R. Iverson, Í. Ö. Benediktsson, A. Schomacker, L. K. Zoet, M. D. Johnson, T. S. Hooyer and Ó. Ingólfsson 2016 Origin of the active drumlin field at Múlajökull, Iceland: new insights from till shear and consolidation patterns. *Quat. Sci. Revs.* **148**, 243–260.
- Meier, S. W., D. A. Melani Barreiro, J. M. Ottino and R. M. Lueptow 2008 Coarsening of granular segregation patterns in quasi-two-dimensional tumblers. *Nature Physics* **4**, 244–248.
- Menzies, J. M. 1979a The mechanics of drumlin formation with particular reference to the change in pore-water content of the till. *J. Glaciol.* **22**, 373–384.
- Menzies, J. 1979b A review of the literature on the formation and location of drumlins. *Earth Sci. Rev.* **14**, 315–359.
- Millis, J. 1911 What caused the drumlins? *Science* **34**, 60–62.
- Möller, P. 2006 Rogen moraine: an example of glacial re-shaping of pre-existing landforms. *Quat. Sci. Revs.*, **25**, 362–389.
- Möller, P. 2010 Melt-out till and ribbed moraine formation, a case study from south Sweden. *Sed. Geol.*, in press. doi: 10.1016/j.sedgeo.2009.11.003.
- Nye, J. F. 1976 Water flow in glaciers: jökulhlaups, tunnels, and veins. *J. Glaciol.* **17**, 181–207.
- Patterson, C. J. and L. H. Hooke 1995 Physical environment of drumlin formation. *J. Glaciol.* **41**, 30–38.
- Pelletier, J. D. 2008 Quantitative modeling of Earth surface processes. C. U. P., Cambridge.
- Röthlisberger, H. 1972 Water pressure in intra- and subglacial channels. *J. Glaciol.* **11**, 177–203.

- Schoof, C. 2007a Pressure-dependent viscosity and interfacial instability in coupled ice-sediment flow. *J. Fluid Mech.* **570**, 227–252.
- Schoof, C. 2007b Cavitation in deformable glacier beds. *SIAM J. Appl. Math.* **67**, 1,633–1,653.
- Sergienko, O. V. and C. L. Hulbe 2011 ‘Sticky spots’ and subglacial lakes under ice streams of the Siple Coast, Antarctica. *Ann. Glaciol.* **52**, 18–22.
- Shaw, J. 1983 Drumlin formation related to inverted melt-water erosional marks. *J. Glaciol.* **29**, 461–479.
- Shaw, J. 1994 Hairpin erosional marks, horseshoe vortices and subglacial erosion. *Sed. Geol.* **91**, 269–283.
- Shaw, J. and D. Kvill 1984 A glaciofluvial origin for drumlins of the Livingstone Lake area, Saskatchewan. *Can. J. Earth Sci.* **21**, 1,442–1,459.
- Shaw, J. and B. Rains 1989 Drumlins and catastrophic glacial floods. *Sed. Geol.* **62**, 177–202.
- Shaw, J. and D. R. Sharpe 1987 Drumlin formation by subglacial meltwater erosion. *Can. J. Earth Sci.* **24**, 2,316–2,322.
- Smalley, I. J. and D. J. Unwin 1968 The formation and shape of drumlins and their distribution and orientation in drumlin fields. *J. Glaciol.* **7**, 377–390.
- Smith, J. D. 1970 Stability of a sand bed subjected to a shear flow of low Froude number. *J. Geophys. Res.* **75**, 5,928–5,940.
- Smith, T. R. and F. P. Bretherton 1972 Stability and the conservation of mass in drainage basin evolution. *Water Resour. Res.* **8**, 1,506–1,529.
- Spagnolo, M., C. D. Clark and A. L. C. Hughes 2012 Drumlin relief. *Geomorphology* **153–154**, 179–191.
- Stokes, C. R., A. C. Fowler, C. D. Clark, R. C. A. Hindmarsh and M. Spagnolo 2013 The instability theory of drumlin formation and its explanation of their varied composition and internal structure. *Quat. Sci. Revs.* **62**, 77–96.
- Sugden, D. E. and B. S. John 1976 *Glaciers and landscape*. Edward Arnold, London.
- Tarr, R. S. 1894 The origin of drumlins. *Amer. Geol.* **10**, 339–362.
- Tucker, G. E. and R. L. Slingerland 1994 Erosional dynamics, flexural isostasy, and long-lived escarpments: a numerical modeling study. *J. Geophys. Res.* **99**, 12,229–12,243.
- Willgoose, G., R. L. Bras and I. Rodríguez-Iturbe 1991 A coupled channel network growth and hillslope evolution model: I. Theory. *Water Resour. Res.* **27**, 1,671–1,684.